Available online at www.sciencedirect.com

SciVerse ScienceDirect

Ceramics International 39 (2013) 3699–3708

CERAMICS INTERNATIONAL

www.elsevier.com/locate/ceramint

Fabrication and mechanical properties of short ZrO_2 fiber reinforced $NiFe_2O_4$ matrix composites

Zhongsheng Hua[a,*], Guangchun Yao[b], Junfei Ma[b], Meiling Zhang[a]

[a]School of Metallurgy and Resources, Anhui University of Technology, Maanshan 243002, China
[b]School of Materials and Metallurgy, Northeastern University, Shenyang 110004, China

Received 13 September 2012; received in revised form 11 October 2012; accepted 12 October 2012
Available online 23 October 2012

Abstract

Short ZrO_2 fibers ($ZrO_{2(f)}$) reinforced $NiFe_2O_4$ ceramic composites were fabricated by cold pressing process. The phase composition, microstructure, mechanical properties and fiber/matrix interface of the composites were investigated by X-ray diffraction, scanning electron microscopy and mechanical testing machines. $ZrO_{2(f)}$ show good thermodynamic and chemical compatibility with $NiFe_2O_4$ ceramic matrix and effectively enhanced the mechanical properties. The toughening mechanisms are fiber bridging, interfacial debonding, fiber pullout, phase transformation and the matrix constraint effect. By incorporation of 3 wt% fibers with the average length of 5∼6 mm, the bending strength and fracture toughness of the composites reached 88.92 MPa and 4.62 MPa $m^{1/2}$, respectively, while the strength conservation ratio after thermal shock increased from 48.85% to 75.86%. The weak interface bonding built up between $ZrO_{2(f)}$ and $NiFe_2O_4$ facilitates the reinforcing effects of the fibers to operate.

Keywords: B. Composites; B. Fibers; C. Mechanical properties; D. ZrO_2

1. Introduction

In conventional aluminum electrolysis using carbon materials as anode, a great deal of high-quality carbon is consumed and quantities of environmental harmful gas such as carbon dioxide and fluorocarbon are discharged. Thus, inert anode [1] has received much attention in the international aluminum industry and materials field due to its advantages including decreasing carbon consumption and eliminating the discharge of greenhouse gas and carcinogenic substances. The search for the material that could serve as an inert anode has taken more than 100 years and the research work mainly focused on three materials classes, namely, metals [2,3], ceramic oxides [4,5], and cermets [6,7]. In these candidate materials, $NiFe_2O_4$ ceramic which is physically stable at service temperature, electrochemically stable and resistant to attack by molten fluoride electrolyte and pure oxygen, becomes one of the most promising materials for inert anode in aluminum electrolysis. But when used as the anode in aluminum electrolysis, in particular, it must be resistant to thermal shock and mechanically robust [1]. It is well-known that aluminum electrolysis is generally conducted at a high temperature of 960∼980 °C, while the poor fracture toughness and thermal shock resistance of $NiFe_2O_4$ ceramic have restricted its application in inert anode materials. The unacceptable drawbacks can be overcome by incorporating particulate, whisker or fiber into the base materials to form ceramic matrix composites [8,9].

Ceramic matrix composites reinforced with fibers [10–14] possess high fracture resistance when the incorporated fibers are intact and the fiber-matrix interface is susceptible to bond and slide under limited stress, however, their strength and toughness are limited by the strong adhesion between fiber and matrix owing to the chemical reaction. Oxide fibers have a distinct chemical advantage over non-oxide fibers for use at high temperatures in oxidizing or corrosive environments. ZrO_2 fiber is a very promising composite reinforcement material that may be applied in many advanced fields because of its high melting point, excellent strength and toughness, low thermal conductivity, super

*Corresponding author. Tel./fax: +86555 2311 571.
E-mail address: huazs83@yahoo.com.cn (Z. Hua).

0272-8842/$ - see front matter © 2012 Elsevier Ltd and Techna Group S.r.l. All rights reserved.
http://dx.doi.org/10.1016/j.ceramint.2012.10.203

corrosion and oxidation resistance, and other fine characteristics [15]. Short ZrO_2 fibers are characterized not only by lower price and good eligible mechanical properties but also by the economic processing methods compared to continuous fibers reinforcement. Using short ZrO_2 fibers, the $ZrO_{2(f)}/NiFe_2O_4$ composites can be well used in the field of inert anode for aluminum electrolysis because of their easy adaptability to conventional manufacturing techniques and then low cost of fabrication. However, reports on fabrication and mechanical properties of short ZrO_2 fibers reinforced $NiFe_2O_4$ composites are very limited.

In present work, ZrO_2 fibers reinforced $NiFe_2O_4$ matrix composites were prepared by cold statistic pressing. The purpose of this paper is to report the processing method and an initial investigation of the microstructure and mechanical properties of $ZrO_{2(f)}/NiFe_2O_4$ composites with different fiber content. In particular, special emphasis is given to demonstrate the effect of ZrO_2 fibers on the mechanical properties of the composites to understand the reinforcing mechanism.

2. Experimental

2.1. Fabrication of $ZrO_{2(f)}/NiFe_2O_4$ composites

The raw materials NiO and Fe_2O_3 powder used in this study were both of reagent grade with the mean particle size of 0.5∼1.0 μm. $NiFe_2O_4$ was synthesized via solid-state sintering technology. A given amount of NiO and Fe_2O_3 were mixed using a ball mill and then calcined in a muffle furnace at 1000 °C for 6 h in air to synthesize $NiFe_2O_4$ ceramic powders. X-ray diffraction spectra of the composites are shown in Fig. 1. The ceramic matrix were composed of $NiFe_2O_4$ and NiO, and contained 10 wt% excess NiO to assure an activity coefficient of 1 for nickel oxide, as this phase has a significantly lower solubility in molten cryolite than Fe_2O_3 [16].

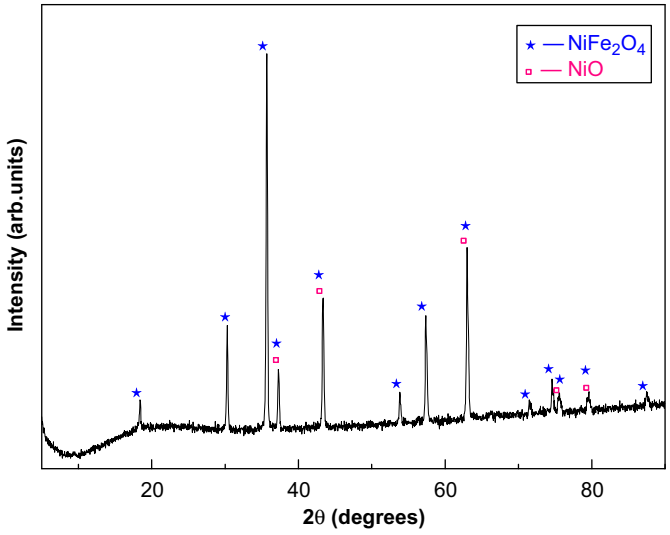

Fig. 1. XRD spectra of $NiFe_2O_4$ ceramic.

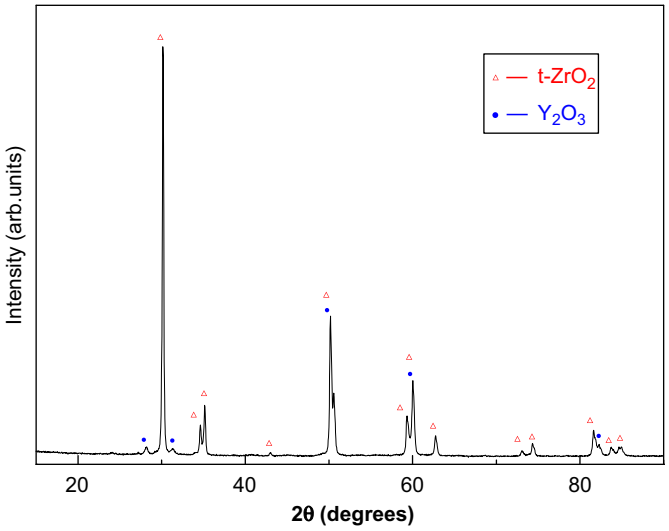

Fig. 2. XRD spectra of $ZrO_{2(f)}$.

Commercial zirconia fibers (Shandong Hongyang Refractory Co., LTD, China) partially stabilized with yttria (about 8.8% in weight fraction) with the medium diameter of 8∼10 μm were employed for the preparation of the composite material in this work. Results of XRD analysis (see Fig. 2) show that the initial $ZrO_{2(f)}$ are mainly composed of tetragonal polycrystalline ZrO_2 and cubic Y_2O_3. Fig. 3 presents SEM micrographs of the surfaces and EDX analysis of $ZrO_{2(f)}$, and some properties of the fibers are summarized in Table 1. The fibers were cut into a length of about 5∼6 mm before fabricating the $ZrO_{2(f)}/NiFe_2O_4$ composites. Firstly, the synthesized $NiFe_2O_4$ powders were ground in distilled water containing adhesive to form the slurry with certain viscosity. Then short $ZrO_{2(f)}$ were added to the slurry under mechanical stirring at a proper speed. The mixed slurries were further stirred for 3 h. The obtained slurries were subsequently dried and aggregates were dispersed manually as required. Finally, the dried blends were cold pressed into rectangular blocks under a pressure of 160 MPa and followed by sintering at 1200∼1400 °C for 6 h. By means of the above processing method the $ZrO_{2(f)}/NiFe_2O_4$ composites with different fiber mass frictions were fabricated.

2.2. Characterization

The bulk density and porosity of the samples were determined using the Archimedes technique with distilled water as the immersing medium at room temperature. Fracture surface as well as microstructure investigation of the matrix, fibers and interface between them were examined by scanning electron microscopy (SEM: SSX-550, Shinadzu Corporation, Japan) at an accelerating voltage of 15 kV. Chemical analysis was performed simultaneously with SEM using energy dispersive X-ray spectroscopy (EDX). The constitution phases of the composites were determined by X-ray diffractometry (XRD: PW3040/60, Panalytical B.V. Corporation, Holand) at a scanning rate of 5°/min using

monochromatic target of Cu-Kα. Differential scanning calorimetry and thermal gravimetric analysis experiments were performed using a simultaneous DSC-TGA instrument (STA 409C/CD, Netzsch, Germany) in air up to 1400 °C with a constant heating rate of 10 °C/min.

2.3. Mechanical testing

Three-point-bending model was used to measure the bending strength over a 30 mm span at a crosshead speed of 0.1 mm/min, using a universal testing machine (INSTRON4206-006, America). Facture toughness measurements were performed on the single-edge notched beam (SENB) specimens using three-point-bending method with a span of 30 mm at the crosshead speed of 0.05 mm/min. The thermal shock resistance was evaluated by placing the samples in a furnace at 960 °C from room temperature and maintaining at 960 °C for 10 min, followed by taking out immediately and cooling to room temperature again in air. Then the retained strength was tested and the residual strength conservation ratio was calculated from the following formula:

$$\eta = \frac{\sigma_r}{\sigma_c} \times 100\% \quad (1)$$

where η is the residual strength conservation ratio of the sample, σ_r is the retained bending strength after thermal shock and σ_c is the bending strength of sample at room temperature without thermal shock. Data for bending strength, fracture toughness, and thermal shock resistance were gathered on five specimens.

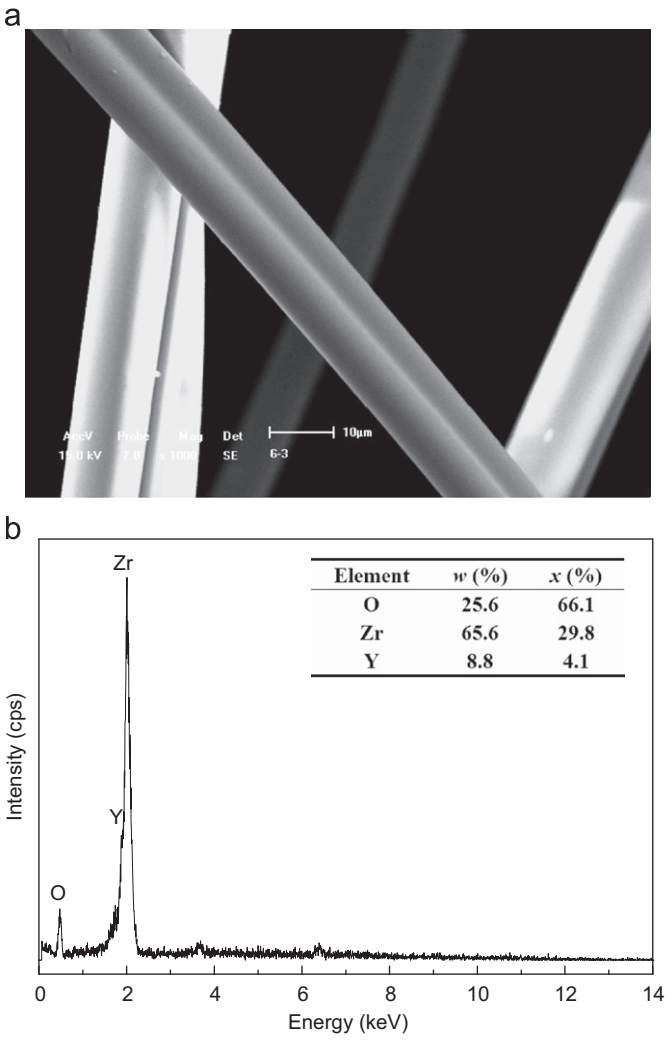

Fig. 3. SEM image (a) and EDX analysis (b) of $ZrO_{2(f)}$.

3. Results and discussion

3.1. Thermodynamic compatibility analysis

The differential scanning calorimeter and thermogravimetry results of $ZrO_{2(f)}/NiFe_2O_4$ green compact before sintering are shown in Fig. 4. If the temperature range gradually increased from room temperature to 1400 °C, the composites just show a little weight loss of 2.28%, which maybe result from: (i) the releasing of water absorbed on the surface of the composites with temperature increasing, (ii) the adsorption and desorption behaviors of oxygen on the surface of the composites and (iii) the burning of some trace impurities of low melting point. It indicates that the composites show a favorable stability at high temperature. Meanwhile, the DSC curve is fairly smooth without any distinct peaks, so it can be inferred from the curve that there are no chemical reactions in the composites during the heating process. From the DSC–TG curves, it is clear that $ZrO_{2(f)}$ can stably exist in $NiFe_2O_4$ ceramic from room temperature to 1400 °C and will not react with the matrix.

$ZrO_{2(f)}/NiFe_2O_4$ composites were fabricated by sintering above 1000 °C. The residual stress will develop inevitably when the composites cool to room temperature due to the difference of the thermal expansion coefficient between $ZrO_{2(f)}$ and $NiFe_2O_4$ matrix. The thermal expansion coefficient of $ZrO_{2(f)}$ between room temperature and 1000 °C is about $13 \times 10^{-6\circ} C^{-1}$, which is slightly higher than that of $NiFe_2O_4$ ceramic ($\sim 10.8 \times 10^{-6\circ} C^{-1}$). The stress that

Table 1
Typical properties of $ZrO_{2(f)}$.

Bulk density (kg m^{-3})	Diameter (μm)	Strength (GPa)	Modulus (GPa)	Melting point (°C)	Thermal expansion coefficient (°C^{-1})
150	8∼10	2.1	340	2677	13×10^{-6}

$ZrO_{2(f)}$ suffered at the interface caused by the thermal expansion mismatch can be described by the following formula:

$$\sigma_f = (\alpha_f - \alpha_m)\Delta T E_f \quad (2)$$

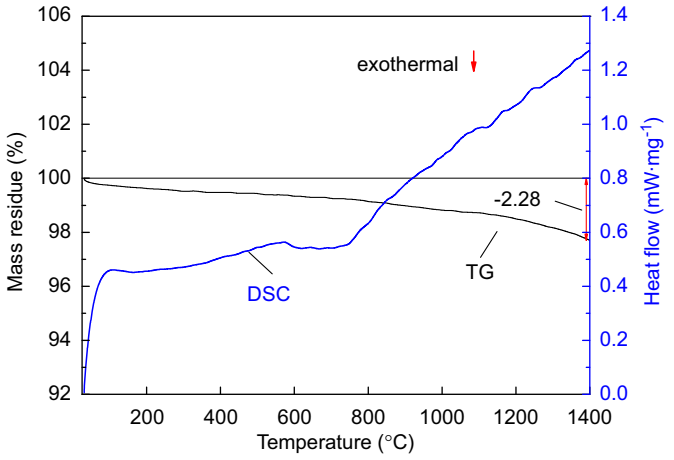

Fig. 4. DSC–TG curves of $ZrO_{2(f)}/NiFe_2O_4$ compact before sintering.

where σ_f is the stress $ZrO_{2(f)}$ suffered at the interface, ΔT is the temperature change during cooling, E_f is modulus of $ZrO_{2(f)}$, α_f and α_m are the thermal expansion coefficients of $ZrO_{2(f)}$ and $NiFe_2O_4$ ceramic, respectively. Since $\alpha_f > \alpha_m$, $ZrO_{2(f)}$ will consequentially suffer the tensile stress. The interface tensile stress will decrease the friction between $ZrO_{2(f)}$ and $NiFe_2O_4$ matrix and make the fibers easy to pullout. More fibers pullout will undoubtedly increase the absorbing energy and benefit the reinforcing effect.

3.2. Densification and phase characterization

The effects of sintering temperature and $ZrO_{2(f)}$ content on the densification of the composites are shown in Fig. 5. It shows that the bulk density increases with increasing sintering temperature and decreases with increasing $ZrO_{2(f)}$ content. The composites containing 3 wt% $ZrO_{2(f)}$ could be densified to 5.13 g cm^{-3} after sintering at 1400 °C for 6 h. The sintering temperature is lower than the melting point of $NiFe_2O_4$ ceramic, so the sintering is attributed to the solid-state reaction, and it mainly depends on the diffusion among the solid particles in this thermally

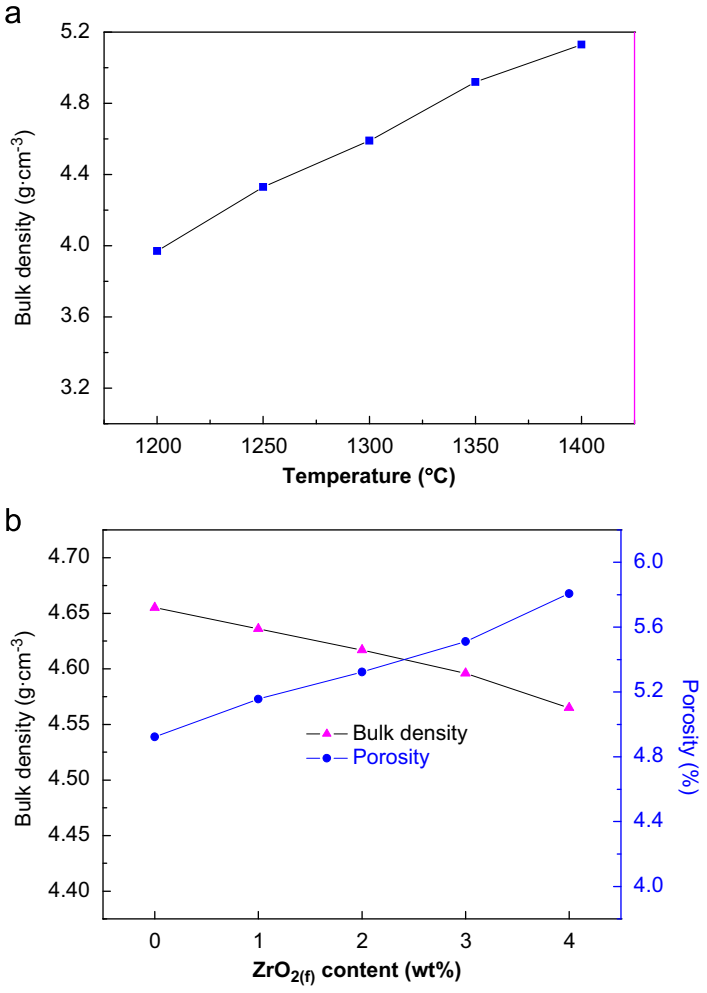

Fig. 5. Densification of the $ZrO_{2(f)}/NiFe_2O_4$ composites as a function of sintering temperature (a) and $ZrO_{2(f)}$ content (b).

activated process. Thus the sintering temperature exhibits decisive effect on densification. The relationship between diffusion coefficient D and temperature T is described as the following equation:

$$D = D_0 \exp\left(-\frac{Q}{RT}\right) \quad (3)$$

where D_0 is the pre-exponential coefficient, Q is the activation energy and R is the gas constant. According to formula (3), the diffusion coefficient shows exponential growth with the increasing sintering temperature, consequently it accelerates the sintering process and leads to the decrease of porosities in $ZrO_{2(f)}/NiFe_2O_4$ composites. In short, increasing sintering temperature can more effectively promote the densification of the composites. But abnormal growth of $NiFe_2O_4$ grains will appear in the composites at exorbitant temperature and results in the decrease of their comprehensive performance.

The effect of adding $ZrO_{2(f)}$ on densification can be described from two aspects. On the one hand, at the given sintering temperature and time, the driving force for sintering is relatively constant, and the mean shear stress in the composites increases due to the presence of $ZrO_{2(f)}$, which results in the decrease of sintering speed. In addition, $ZrO_{2(f)}$ decrease the mass transfer rate and counteract the discharge of porosities, while the fibers contacting also leads to the density decrease of the composites. Thus, the bulk density of the composites decreases with the increasing $ZrO_{2(f)}$ content. Generally, the relationship between bending strength and porosity of $ZrO_{2(f)}/NiFe_2O_4$ composites can be illustrated by Ryskewitsch's empirical formula

$$\sigma = \sigma_0 \exp(-nP) \quad (4)$$

where σ is the strength of the composites with porosity of P, σ_0 is the strength for composites without pores, and n is a constant. A similar effect has been also observed in short fiber reinforced TiC, ZrB_2 and $BaSi_2Al_2O_8$ (BAS) composites [9,17,18].

On the other hand, yttria partially stabilized ZrO_2 has an effect on grain refining [19]. Fig. 6 shows the fractured surface of the specimens for testing fracture toughness. The growth of $NiFe_2O_4$ grains was inhibited due to the existence of short $ZrO_{2(f)}$, and thus led to the decrease of the average grain size. Hall–Pitch formula has illustrated the relationship between the strength and grain size of ceramic materials

$$\eta = \eta_0 + Kd^{-\frac{1}{2}} \quad (5)$$

where η is the strength of ceramic materials, d is the grain size, η_0 and K are constants. Formula (5) has indicated that the decrease of $NiFe_2O_4$ grain size after adding $ZrO_{2(f)}$ is beneficial for improving the mechanical properties of the composites.

Since the temperature is the key influencing factor of phase transformation, it is necessary to investigate the effect of different sintering temperatures on the phase of the composites. XRD patterns of the composites containing 3 wt% $ZrO_{2(f)}$ sintered at 1200∼1400 °C are shown in Fig. 7. The XRD structures of $ZrO_{2(f)}/NiFe_2O_4$ composites sintering at different temperature are fairly similar. It reveals that only $NiFe_2O_4$, NiO, ZrO_2 and Y_2O_3 as crystalline phases present in the composites, and no other phases are detected, which confirms that $ZrO_{2(f)}$ can stably

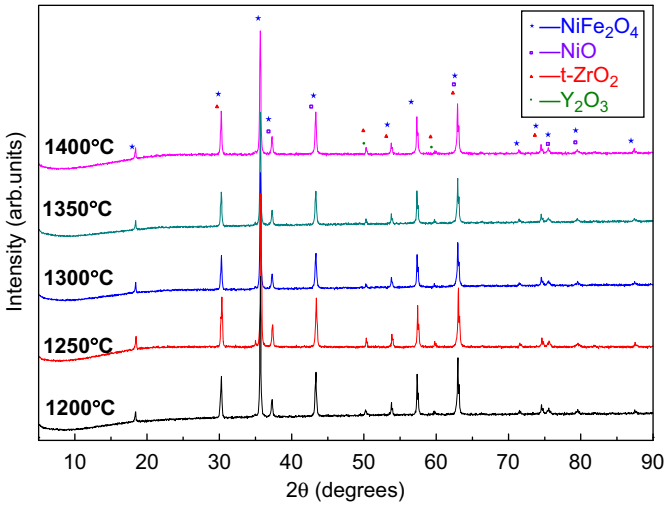

Fig. 7. XRD spectra of the composites containing 3 wt% fibers after sintering at different temperature.

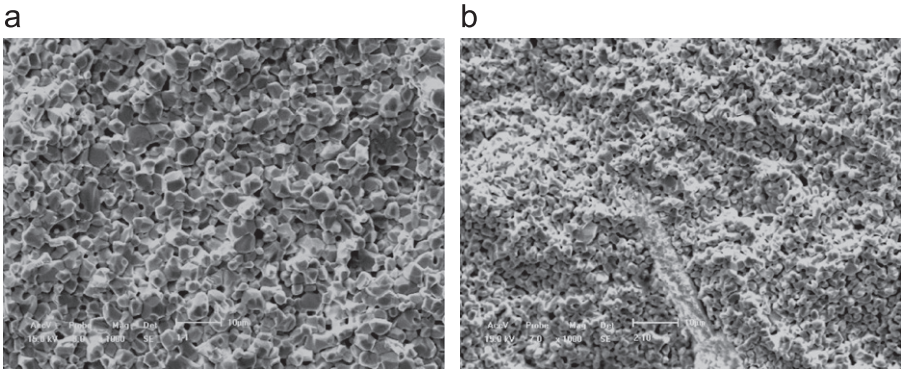

Fig. 6. SEM images of the fracture surface of specimens (a) without and (b) with adding $ZrO_{2(f)}$.

exist in $NiFe_2O_4$ ceramic and not react with the matrix at high temperature. It is in excellent agreement with the results of DSC–TG analysis.

3.3. Microstructure characterization

Fig. 8 represents the typical microstructures for the fracture surfaces perpendicular to the direction of loading during pressing for specimens with different fiber content sintering at 1300 °C for 6 h. From these micrographs, it is clear that $ZrO_{2(f)}$ homogeneously distribute in continuous $NiFe_2O_4$ matrix and mostly align within planes perpendicular to the pressing direction for the strength of the longitudinal direction is expected to be higher than that of the transverse direction in the unidirectional short-fiber-reinforced composites [20]. Meanwhile, the length of the fibers remarkably changed after mixing and pressing processes. When $ZrO_{2(f)}$ were blended in $NiFe_2O_4$ slurry under high-speed mechanical stirring, lots of them were damaged to short fibers and some ZrO_2 particulates flaked off from the fibers. In addition, some fibers fractured resulting from the volume shrinkage of the green bodies during cold statistic pressing. Thus, the length of $ZrO_{2(f)}$ is much shorter than the original length, and some ZrO_2 particulates are present in the composites, as shown in Fig. 8.

When $ZrO_{2(f)}$ are well distributed in $NiFe_2O_4$ ceramic matrix, there are no obvious air pores and holes present in the composites. In addition, according to the bulk density variation shown in Fig. 5(b), the microstructure should appear to be denser for the $NiFe_2O_4$ ceramic with lower fiber content, but because the porosities of $ZrO_{2(f)}/NiFe_2O_4$ composites are all below 6%. This implies that the relative densities of the composites are all above 94%, and it is hard to distinguish the differences in the microstructure of specimens with different fiber additions from each other in Fig. 8(a)–(d).

3.4. Mechanical properties of the composites

The mechanical properties of the $ZrO_{2(f)}/NiFe_2O_4$ composites with different fiber addition are shown in Fig. 9. All the bending strength, fracture toughness and strength retention after thermal shock increase with $ZrO_{2(f)}$ content increasing from 0 to 3 wt%. The bending strength and fracture toughness of the composites containing 3 wt% $ZrO_{2(f)}$ reach 88.92 MPa and 4.62 MPa $m^{1/2}$, increasing 32.6% and 80.5% compared to the pure $NiFe_2O_4$ matrix, respectively, while the strength conservation ratio after thermal shock increases from 48.85% to 75.86%.

The bending strength and the fracture toughness show the similar tendency. Improvement in mechanical properties of the composites can be attributed to the good interfacial bonding between $ZrO_{2(f)}$ and $NiFe_2O_4$, which has effectively realized the load to transfer from the matrix to fibers. As reinforcement, the strength of zirconia fiber is far higher than that of matrix, that is $\sigma_f > \sigma_m$. According to the following rule-of-mixture formulation:

$$\sigma_c = \sigma_f C V_f + \sigma_m (1 - V_f) \quad (6)$$

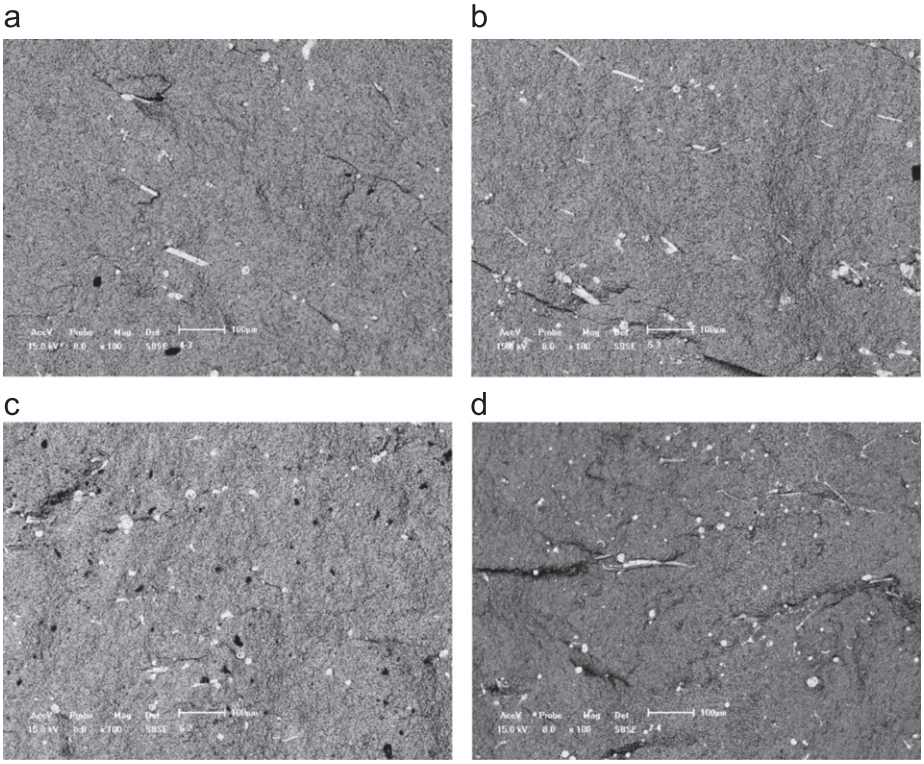

Fig. 8. SEM images of $ZrO_{2(f)}/NiFe_2O_4$ composites with different fiber content: (a) 1 wt%, (b) 2 wt%, (c) 3 wt%, and (d) 4 wt%.

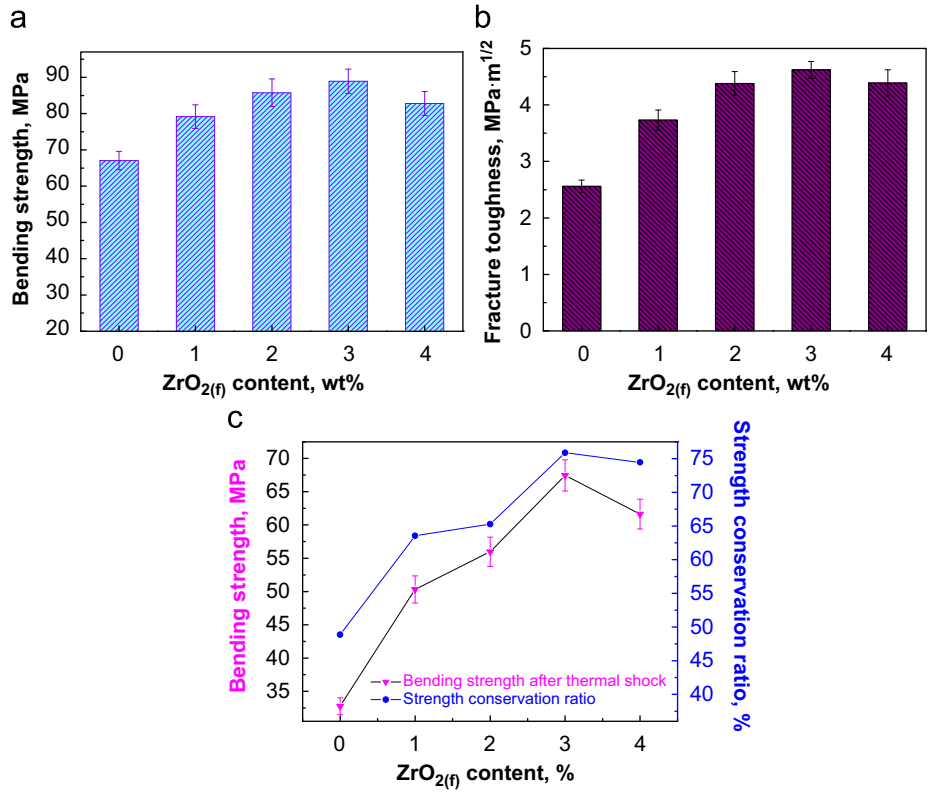

Fig. 9. Mechanical properties of the $ZrO_{2(f)}/NiFe_2O_4$ composites as a function of $ZrO_{2(f)}$ content: (a) bending strength, (b) fracture toughness, and (c) thermal shock resistance.

where σ_c, σ_f and σ_m are the strengths of the composites, fiber and matrix, respectively, V_f is the fiber volume content and C is a constant, the strength of the composites will increase as the fiber content is increased. This is true in low fiber content. But the case is quite different at excessively high $ZrO_{2(f)}$ content. When the addition is up to a high value, $ZrO_{2(f)}$ are likely to distribute in fasciculate, thus more pores will generate. In this case, the porosity dominates the mechanical properties of the composites. From Fig. 5 and Eq. (4), the composites with higher fiber content consequently have higher porosity, and thus the strength of the composites decreases with the increase of fiber content. Moreover, the interlacement of $ZrO_{2(f)}$ increased the defects in $ZrO_{2(f)}/NiFe_2O_4$ composites, which results in the poor load transfer, weakening the reinforcing effect and decreasing the strength of the composites [13]. Even if the fiber content is up to 4 wt%, the composites show higher mechanical properties than the pure $NiFe_2O_4$ ceramic. That probably results from the decrease in grain size.

As for the improvement in thermal shock resistance, it is probably attributed not only to the increase of toughness but also to the proper porosities in the composites. The porosities have a certain effect on blunting cracks and decreasing the stress concentration in composites. On the contrary, the ceramic materials with excessively high density are prone to cracking when they suffer thermal shock. In this sense, proper porosities in $ZrO_{2(f)}/NiFe_2O_4$ composites are beneficial to the thermal shock resistance. Therefore, only adding the moderate amount of the fibers can improve the mechanical properties of $ZrO_{2(f)}/NiFe_2O_4$ composites. In this study, the $ZrO_{2(f)}/NiFe_2O_4$ composites with fiber mass content of 3% possess good integrative properties.

3.5. Toughening mechanisms analysis

When moderate amount of $ZrO_{2(f)}$ with proper length are incorporated and uniformly distributed in $NiFe_2O_4$ matrix, the experimental results above show that the mechanical properties of $ZrO_{2(f)}/NiFe_2O_4$ composites can be significantly improved. At first, the toughening mechanisms of $ZrO_{2(f)}/NiFe_2O_4$ composites can be deduced from the SEM observation of the fracture surface of specimens, as shown in Fig. 10. Obviously, the reinforcing mechanisms are fiber pullout, interface debonding and fiber bridging. When the composites begin to fracture under external load, the front of crack propagates beyond $ZrO_{2(f)}$, the intact fibers bridge the fracture surface in the wake of the crack, thus the open displacement of the crack is limited and further propagation of the crack become difficult. As a result, the cracks are arrested by $ZrO_{2(f)}$ and some of them deflect at the fiber/matrix interface resulting in fiber debonding. Moreover, many holes formed on the surface, which are resulted from the fiber pullout. While the load transfers from $NiFe_2O_4$ matrix to $ZrO_{2(f)}$ and the fiber/matrix interface adhesion is

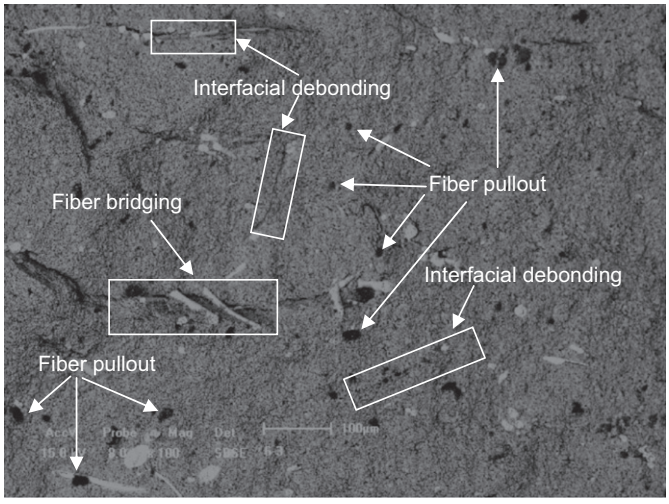

Fig. 10. SEM image of the fracture surface of $ZrO_{2(f)}/NiFe_2O_4$ composites.

relatively low, and the fibers would be pulled out. During fiber bridging, interface debonding and fiber pullout, much higher fracture energy is consumed and thus the bending strength and fracture toughness are improved to prevent the catastrophic failure under external force.

As we all know, yttria partially stabilized tetragonal zirconia can exist at ambient temperatures [21] and has superior fracture toughness owing to the stress-induced martensitic phase transformation from tetragonal ($t-ZrO_2$) to monoclinic phase ($m-ZrO_2$) in the stress field of propagating cracks [22]. $ZrO_{2(f)}$ have the virtue of phase transformation toughening as well as fiber-toughening. As mentioned above, $ZrO_{2(f)}$ were deformed during the processes of mixing and molding and some zirconia particles were desquamated in $NiFe_2O_4$ ceramics. Although $ZrO_{2(f)}$ lose the effect of fiber-toughening when they are broken to particles, the zirconia particles still have the toughening effect of phase transformation [21,23]. In the mechanism of transformation toughening, the stresses at the crack tip in $ZrO_{2(f)}/NiFe_2O_4$ composites would transform the metastable tetragonal phase to monoclinic phase resulting in volume increase of about 4∼5% [21,24]. Fig. 11 reveals that m-ZrO_2 exists at the fractured surface of the composites. Volume increase generates compressive stresses in the vicinity of the crack tip and thus arrests crack propagation. This effect of volume increase is also responsible for the toughening of $ZrO_{2(f)}/NiFe_2O_4$ composites. The toughness of a zirconia-toughened $ZrO_{2(f)}/NiFe_2O_4$ composites, $K_{IC,C}$, is composed of the matrix toughness, $K_{IC,matrix}$, and a toughness enhancement, ΔK_{IC}, attributed to the phase transformation as follows:

$$K_{IC,C} = K_{IC,matrix} + \Delta K_{IC} \quad (7)$$

Furthermore, the matrix constraint effect is also beneficial to toughness enhancement. As described previously, thermal residual stress will build up at the fiber/matrix interface when the $ZrO_{2(f)}/NiFe_2O_4$ composites cool from sintering temperature to room temperature, and the ceramic matrix is subjected to the compressive stress for its thermal expansion coefficient is lower than that of $ZrO_{2(f)}$. This stress can restrict the composites to fracture under external load, resulting in the improvement of strength and toughness.

3.6. Interface analysis

Like other brittle matrices, the $NiFe_2O_4$ ceramic can be toughened by short fibers. Nevertheless, the toughening effect is dramatically dependent on the nature and strength of fiber/matrix interface, which is the key element transferring the load from the matrix to the fibers. The typical interface micrograph of $ZrO_{2(f)}/NiFe_2O_4$ composites is shown in Fig. 12. It is clear that there is no interfacial layer resulting from chemical reaction, and exist distinct little gap between the fiber and the matrix, which is undoubtedly due to thermal coefficient mismatch of the

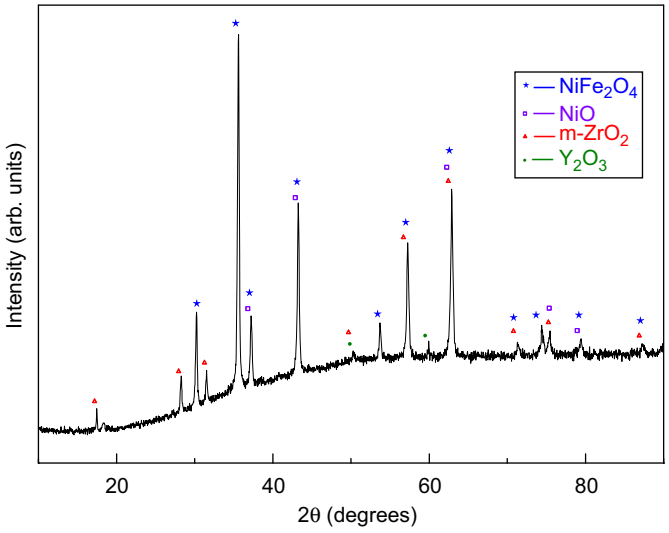

Fig. 11. XRD spectra of the fracture surface of $ZrO_{2(f)}/NiFe_2O_4$ composites.

Fig. 12. A typical interface micrograph of $ZrO_{2(f)}/NiFe_2O_4$ composites.

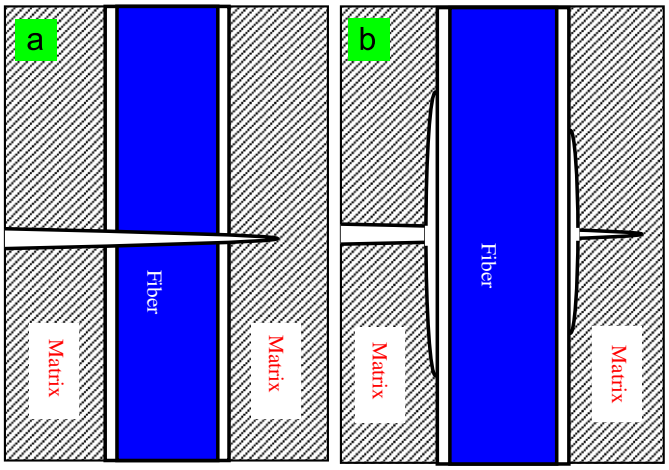

Fig. 13. Sketch diagraphs of fiber/matrix composites with (a) strong and (b) weak interfacial bonding.

two materials. The weak $ZrO_{2(f)}/NiFe_2O_4$ interfacial bonding will result in a trend for $ZrO_{2(f)}$ debonding during cooling. In particular, $ZrO_{2(f)}$ remain in good condition with relatively coarse and intact surface after sintering at 1300 °C for 6 h, which further indicates that $ZrO_{2(f)}$ exhibit a good chemical compatibility with the investigated ceramic matrix. The results from SEM observation are quite consistent with the DSC–TG and XRD analyses.

The fiber/matrix interface adhesion is not expected to be stronger than the strength of the matrix. Otherwise, composites will fail prematurely at the fiber/matrix interface before the load-carrying capability of the fibers is fully developed. Weak fiber/matrix interfacial bonding in a brittle matrix composites is responsible for transferring the applied load onto the load bearing fibers, thus facilitating toughening mechanisms such as interfacial debonding and fiber pullout to operate. As demonstrated in Fig. 13, when the interfacial bonding is weak, the crack propagates along the tortuous path on the interface therefore more energy is absorbed. In contrast, a strong interfacial bonding tends to allow a crack to propagate straightly through the fibers, and the fibers lose their effect on bridging, which results in low fracture toughness [25,26]. The weak interfacial bonding built up between $ZrO_{2(f)}$ and $NiFe_2O_4$ was beneficial for the reinforcing effects to operate. Therefore, it can be concluded that $ZrO_{2(f)}$ are the ideal reinforcements for $NiFe_2O_4$ ceramic.

4. Conclusions

Short $ZrO_{2(f)}$ reinforced $NiFe_2O_4$ ceramic composites were fabricated by cold statistic pressing, followed by sintering at 1200∼1400 °C. The composites possess higher bending strength, higher fracture toughness, better thermal shock resistance and slightly lower density compared to pure $NiFe_2O_4$. Through the mechanical properties investigation and the reinforcing effect and interface analyses, several helpful conclusions have been reached as follows.

1. $ZrO_{2(f)}$ exhibit good thermodynamic and chemical compatibility with $NiFe_2O_4$ matrix at high temperature. Tensile stresses develop at the fiber/matrix interface because the radial thermal expansion coefficient of $ZrO_{2(f)}$ is slightly larger than that of $NiFe_2O_4$. The tensile strength at the interface makes the fiber pull-out easy, thus is beneficial to enhance the mechanical properties of the composites.
2. The bulk density of $ZrO_{2(f)}/NiFe_2O_4$ composites increases with increasing sintering temperature and sintering time. The relative densities of the composites sintering at 1300 °C for 6 h are all above 94%, and there are no obvious differences in the microstructure of specimens with different fiber additions.
3. The mechanical properties of $NiFe_2O_4$ matrix can be greatly improved by adding $ZrO_{2(f)}$ when they are well distributed. By incorporation of 3 wt% fibers, the bending strength and fracture toughness of the composites reach 88.92 MPa and 4.62 MPa $m^{1/2}$, increasing 32.6% and 80.5% compared to the pure $NiFe_2O_4$ matrix, respectively, while the strength conservation ratio after thermal shock increases from 48.85% to 75.86%.
4. $ZrO_{2(f)}$ are the ideal reinforcements for $NiFe_2O_4$ ceramic. The reinforcing mechanisms in $ZrO_{2(f)}/NiFe_2O_4$ composites are mainly fiber bridging, interfacial debonding, fiber pullout, phase transformation and the matrix constraint effect. The weak interfacial bonding built up between $ZrO_{2(f)}$ and $NiFe_2O_4$ facilitates the reinforcing effects to operate.

Acknowledgments

The authors are grateful for the financial support from National Natural Science Foundation of China (Nos. 51204002 and 50834001).

References

[1] D.R. Sadowy, Inert anodes for the Hall-Héroult cell: the ultimate materials challenge, Journal of the Minerals, Metals and Materials Society 53 (2001) 34–35.
[2] M. Glucina, M. Hyland, Laboratory-scale performance of a binary Cu–Al alloy as an anode for aluminium electrowinning, Corrosion Science 48 (2006) 2457–2469.
[3] Z. Shi, J. Xu, Z Qiu, Z. Wang, Copper–nickel superalloys as inert alloy anodes for aluminum electrolysis, Journal of the Minerals, Metals and Materials Society 55 (2003) 63–65.
[4] E. Olsen, J. Thonstad, Nickel ferrite as inert anodes in aluminium electrolysis Part II: material performance and long-term testing, Journal of Applied Electrochemistry 29 (1999) 301–311.
[5] H. Xiao, R. Hovland, S. Rolseth, J. Thonstad, Studies on the corrosion and the behavior of inert anodes in aluminum electrolysis, Metallurgical and Materials Transactions B 27 (1996) 185–193.
[6] Y. Lai, X. Sun, J. Li, H. Duan, X. Li, G. Zhang, Z. Tian, Densification of Ni–$NiFe_2O_4$ cermets for aluminum electrolysis, Transactions of Nonferrous Metals Society of China 15 (2005) 666–670.

[7] Y. Lai, Z. Tian, J. Li, S. Ye, X. Li, Y. Liu, Results from 100h electrolysis testing of $NiFe_2O_4$ based cermet as inert anode in aluminum reduction, Transactions of Nonferrous Metals Society of China 16 (2006) 970–974.
[8] X.B. He, X.M. Zhang, C.R. Zhang, X.G. Zhou, A.N. Zhou, Microstructures and mechanical properties of C_f/SiC composites by precursor pyrolysis-hot pressing, Materials Science and Engineering A: Structural Materials Properties Microstructure and Processing 284 (2000) 211–218.
[9] W.G. Fahrenholtz, G.E. Hilmas, A.L. Chamberlain, J.W. Zimmermann, Processing and characterization of ZrB_2-based ultra-high temperature monolithic and fibrous monolithic ceramics, Journal of Materials Science 39 (2004) 5951–5957.
[10] F. Yang, X. Zhang, J. Han, S. Du, Mechanical properties of short carbon fiber reinforced ZrB_2-SiC ceramic matrix composites, Materials Letters 62 (2008) 2925–2927.
[11] F. Ye, L. Liu, L. Huang, Fabrication and mechanical properties of carbon short fiber reinforced barium aluminosilicate glass-ceramic matrix composites, Composites Science and Technology 68 (2008) 1710–1717.
[12] Z.B. Yu, D.P Thompson, A.R. Bhatti, Fabrication and characterisation of SiC fibre reinforced lithium-α-sialon matrix composites, Composites Part A: Applied Science and Manufacturing 33 (2002) 621–629.
[13] H. Tang, X. Zeng, X. Xiong, L. Li, J. Zou, Mechanical and tribological properties of short-fiber-reinforced SiC composites, Tribology International 42 (2009) 823–827.
[14] M.C. Wang, Z.G. Zhang, Z.J. Sun, M. Li, Effect of fiber type on mechanical properties of short carbon fiber reinforced B_4C composites, Ceramics International 35 (2009) 1461–1466.
[15] H.Y. Liu, X.Q. Hou, X.Q. Wang, Y.L. Wang, D. Xu, C. Wang, W. Du, M.K. Lv, D.R. Yuan, Fabrication of high-strength continuous zirconia fibers and their formation mechanism study, Journal of the American Ceramic Society 87 (2004) 2237–2241.
[16] E. Olsen, J. Thonstad, Nickel ferrite as inert anodes in aluminium electrolysis Part I: material fabrication and preliminary testing, Journal of Applied Electrochemistry 29 (1999) 293–299.
[17] F. Yang, X. Zhang, J. Han, S. Du, Processing and mechanical properties of short carbon fibers toughened zirconium diboride-based ceramics, Materials & Design 29 (2008) 1817–1820.
[18] G. Song, Y. Wu, Q. Li, Elevated temperature strength and thermal shock behavior of hot-pressed carbon fiber reinforced TiC composites, Journal of the European Ceramic Society 22 (2002) 559–566.
[19] A.K. Bhattacharya, Microstructure and mechanical properties of 2.5 yttria partially stabilized zirconia-reinforced molybdenum disilicide composites, Journal of Materials Science Letters 12 (1993) 372–375.
[20] E.D. Kragness, M.F. Amateau, G.L. Messing, Processing and characterization of laminated SiC whisker reinforced Al_2O_3, Journal of Composite Materials 25 (1991) 416–432.
[21] B. Basu, Toughening of yttria-stabilised tetragonal zirconia ceramics, International Materials Reviews 50 (2005) 239–256.
[22] A. Mukhopadhyay, B. Basu, S.D. Bakshi, S.K. Mishra, Pressureless sintering of ZrO_2-ZrB_2 composites: microstructure and properties, International Journal of Refractory Metals and Hard Materials 25 (2007) 179–188.
[23] B. Basu, J. Vleugels, O.V. Biest, Toughness tailoring of yttria-doped zirconia ceramics, Materials Science and Engineering A 380 (2004) 215–221.
[24] I. Denry, J.R Kelly, State of the art of zirconia for dental applications, Dental Materials 24 (2008) 299–307.
[25] S.M. Dong, Y. Katoh, A. Kohyama, S.T. Schwab, L.L. Snead, Microstructural evolution and mechanical performances of SiC/SiC composites by polymer impregnation/microwave pyrolysis (PIMP) process, Ceramics International 28 (2002) 899–905.
[26] X. He, Y. Zhou, D. Jia, Y. Guo, Effect of sintering additives on microstructures and mechanical properties of short-carbon-fiber-reinforced SiC composites prepared by precursor pyrolysis-hot pressing, Ceramics International 32 (2006) 929–934.